LLRF SYSTEM DESIGN AND PERFORMANCE FOR XFEL CRYOMODULES CONTINUOUS WAVE OPERATION

J. Branlard*, V. Ayvazyan, Ł. Butkowski, H. Schlarb, J. Sekutowicz, DESY, Hamburg, Germany
W. Cichalewski, A. Piotrowski, K. Przygoda, DMCS, Łódź, Poland
W. Jałmużna, EicSys GMBH, Poland, J. Szewiński, NCBJ, Świerk, Poland

Abstract

The cryomodule test bench (CMTB) at the Deutsches Elektronen Synchrotron (DESY) in Hamburg is equipped with a 100 kW inductive output tube (IOT) allowing the test of superconducting cryomodules in continuous wave (CW) operation mode. Although significantly different from the nominal pulsed operation mode of the European x-ray free electron laser (XFEL), CW operation can be handled by the same low-level radio frequency (LLRF) system, within minor firmware modifications. The hardware details of the LLRF setup at CMTB, the firmware and software architecture and performance results from the last CW test are presented in this contribution.

INTRODUCTION

Benefits of CW Operation

While the currently planned mode of operation of the European XFEL is pulsed, there are clear advantages of running such an accelerator in CW mode [1]. Continuous power usage is more efficient compared to the planned 1.3 msec RF pulse width at a 10 Hz repetition rate. Moreover, the CW mode of operation provides a great flexibility for the beam time structure. Lasers can operate at a lower repetition rate, relaxing the time resolution constrains on the experiment detectors. Finally, transient detuning effects caused by Lorentz forces at each RF pulse no longer are an issue.

Tests are regularly carried at DESY in CMTB on the XFEL prototype cryomodules, to better understand the potential of operating these modules in CW. Instead of the 10 MW klystron, a 100 kW IOT shown in Fig. 1 is used to power the cryomodule. Details about the outcome of the recent first and second CW tests can be found in [2, 3].

Challenges of CW Operation

Powering continuously superconducting cavities with RF yields higher dynamic heat loads, which should be monitored closely and maintained within the cooling capability of the cryogenic system. For XFEL cryomodules, the total acceptable heat load is 20W, including 3-4W static heat load. In order to achieve the highest possible gradient within the cryogenic cooling margin, the cryomodule can also be operated in so-called long-pulse (LP) mode, where the power-on duty factor ranges from 10% up to 50%.

To maximize the power coupling into the cavities, their loaded quality factor (Q_L) is adjusted to 1.5×10^7 from the pulsed mode nominal 3×10^6 value. With this new coupling, 18 kW IOT power are sufficient to achieve 12 MV/m gradient per cavity, compared to about 100 kW for $Q_L = 3 \times 10^6$. As a by-product of this higher coupling, the cavity bandwidth is also reduced: $f_{1/2} \approx 44$ Hz (from nominal 216 Hz), making it more sensitive to external mechanical vibrations or cryogenic pressure fluctuations. Hence in CW and LP mode, microphonics are the dominant source of detuning, but can be compensated for using the piezo-based cavity tuning system.

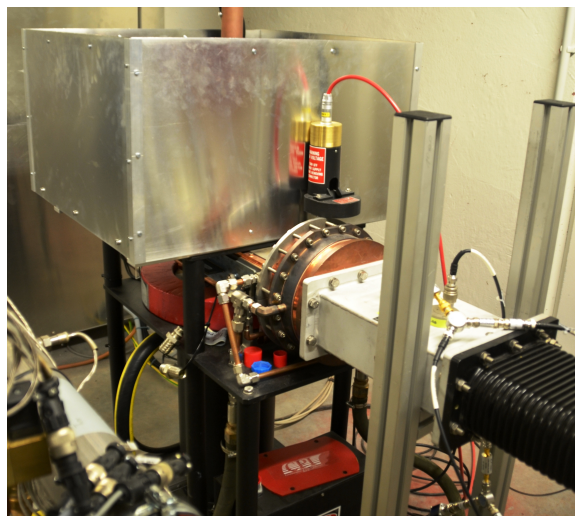

Figure 1: 100 kW Inductive Output Tube.

LLRF SYSTEM OVERVIEW

Hardware Overview

The LLRF system hardware is identical for short pulse, LP or CW operations. Its main components are depicted in Fig. 2. For every cavity, the forward (PFWD), reflected (PREF) and transmitted signals or probes (PRB) are first down-converted to an intermediate frequency (IF) by the down-converters (uDWC) and then digitized (uADC) at 81.25 MHz. The sampled signals are pre-processed by the uADC and then sent over the MTCA.4 backplane to the main LLRF controller (uTC) which performs all control computations. The uTC then generates the drive signal which is up-converted to RF frequency by the vector modulator (uVM). The LLRF drive signal is pre-amplified and then sent to the IOT. The 1.3 GHz RF signal is equally distributed to all cavities through the same waveguide distribution system used for normal pulsed operations.

* julien.branlard@desy.de

ISBN 978-3-95450-143-4

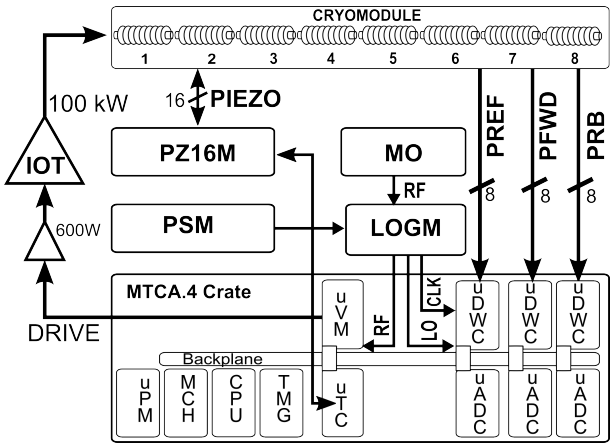

Figure 2: LLRF system block diagram.

The master oscillator (MO) provides the 1.3 GHz reference signal (RF), required by the local oscillator generation module (LOGM) to generate the LO and clocks (CLK) signals used by the down-converters, and to distribute the reference signal to the uVM. The power supply module (PSM) provides DC voltages to external modules. Finally, the piezo driver module (PZ16M) digitizes the piezo sensor data and drives the piezo actuator for detuning and microphonics compensation. Communication between the PZ16M and the MTCA.4 system is performed through an optical link to the main LLRF controller, the uTC. More details about specific MTCA.4 modules (power: uPM, controller hub: MCH, computing unit: CPU, timing: TMG) and the MTCA.4-based LLRF system can be found in [4].

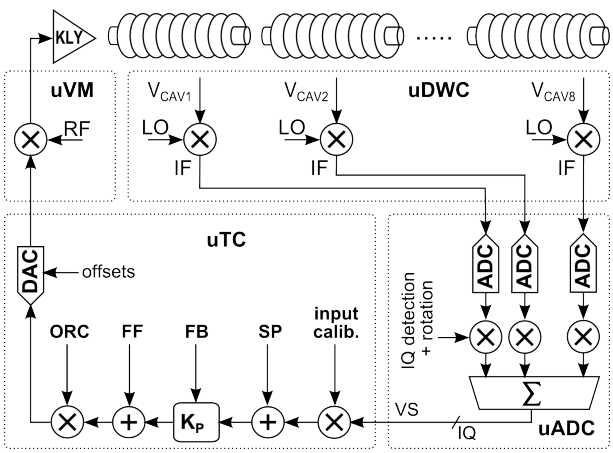

Figure 3: RF feedback control loop.

Firmware Overview

From a controls point of view, two feedback (FB) loops are in action during CW operations: the RF control and the piezo control FB. The RF FB (Fig. 3) is based on a vector-sum (VS) approach, where the sum of all cavity gradients is calculated inside the uADC. This vector-sum is sent to the uTC and compared to a set-point (SP). In-phase and quadrature (IQ) errors are used by a proportional controller to generate the drive signal. After adding the feed-forward table (FF), the controller output signal is scaled in amplitude and phase (output rotation correction, ORC) before the RF up-conversion stage, taking place at the uVM. Undesired carrier signal leakage coming from the up-conversion can be suppressed by adjusting the DC offsets on the controller output DACs.

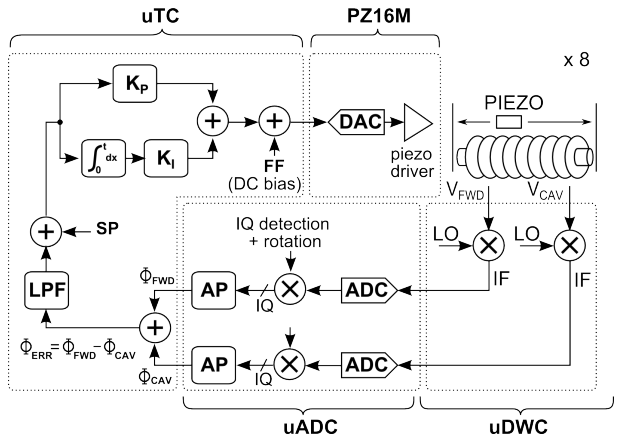

Figure 4: Piezo feedback control loop.

The uADC also computes amplitude and phase (AP) from the digitized cavity IQ signals (Fig. 4). The phases from the forward signals (Φ_{FWD}) and from the cavity probes (Φ_{CAV}) are then sent over the backplane to the main controller, along with the vector-sum at 9.028 MHz.

For every cavity, the piezo FB controller computes the phase difference between the forward signal and the cavity probe: $\Phi_{ERR} = \Phi_{FWD} - \Phi_{CAV}$. The cavity detuning is proportional to this phase difference and is used as input to a PI controller (k_P,k_I). The piezo DC bias are then applied as a FF offset before being sent to the DACs and the piezo driver (PZ16M).

Software Overview

From the LLRF server perspective, interrupts are sent by the timing module to the CPU, triggering the data acquisition at a repetition rate between 1 and 10 Hz. DMA transfers are then taking place over the backplane, with a maximum size of one million samples per transfer. The rate of the sampled data can be adjusted by writing to a register on the controller and on the uADC boards. For CW operations, the repetition rate is set to 1 Hz, the sample rate to 1 MHz so that a one million sample DMA transfer corresponds to a one second data interval. For LP operations, the averaged sampling rate is simply increased (up to 9.028 MHz). The DMA transfer size remains the same, only the data acquisition window size gets reduced.

RESULTS

The performance of the RF controller is illustrated in Fig. 5, showing the CW amplitude vector-sum with and

without FB. The measured in-loop standard deviation deviation is improved by a factor of 25, corresponding to an in-loop RMS regulation of 6×10^{-5} in amplitude and in $0.0098°$ in phase (not shown).

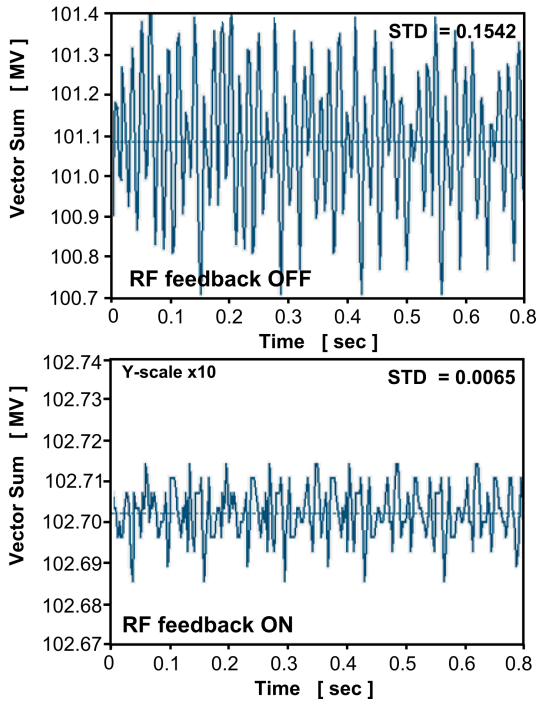

Figure 5: Vector sum amplitude without and with RF feedback in CW mode.

The piezo feedback performance is illustrated in Fig. 6, where the piezo controller error signal (i.e. $\Phi_{CAV} - \Phi_{FWD}$) is shown for a 700 msec pulse. Without feedback (upper), the observed phase roll is dominated by the IOT modulator during the fill time and corresponds to approximately 60-70 Hz. With piezo FB on (lower), the detuning is reduced to less than 2 Hz. Instabilities in the controller error are clearly starting to appear, indicating that the applied piezo feedback gain was marginally stable. Vacuum pumps installed closed to cavity 1 and 8 also introduced external vibrations visible on the plot. This ≈50 Hz component was only damped by a factor of 2 due to bandwidth limitations of the piezo feedback, which can be improved by software.

Open Points

One difficulty encountered during the tests is related to the two concurrent feedback loops. The RF feedback maintains the vector-sum of all cavity gradient to the amplitude and phase set-points, by acting on the forward signal. The piezo feedback maintains the cavity phase in line with the forward phase. These two loops become unstable as the cavity forward phase drifts away from its zero set-point. To better understand the limitations due to the combined use of these two feedback loops, one needs to determine the closed loop bandwidth of the piezo feedback. This was not possible until recently, when the piezo controller firmware

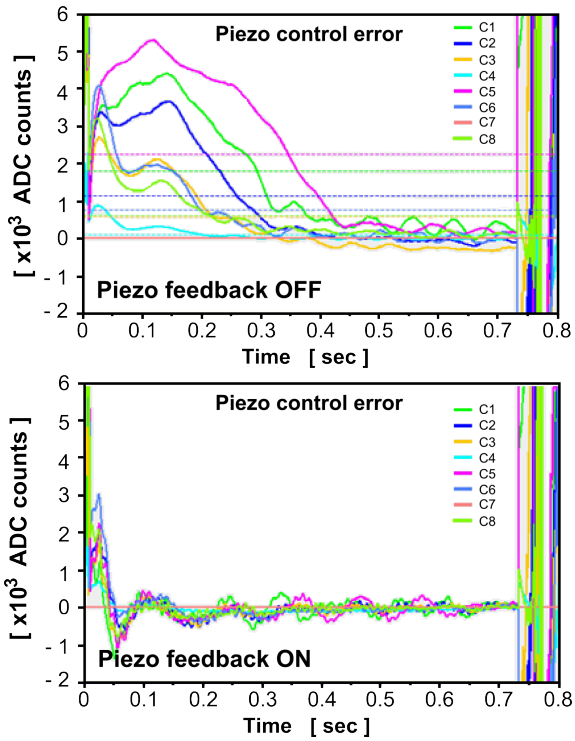

Figure 6: Piezo controller error signal for 8 cavities, with feedback off and on in LP mode.

was updated to allow playing arbitrary waveforms. An impulse response can then be measured and the close loop bandwidth can be computed. This will be tested during the upcoming CW test in Fall 2013. Finally, the controller input low pass filter shown in Fig. 4 had not been implemented at the time of the previous test. This filter should help with the stability of the piezo FB, allowing to operate at higher gains and improving the detuning noise rejection in closed loop operation.

CONCLUSIONS

An overview of the MTCA.4 based LLRF system used for CW and LP test was given. Preliminary results show controller performances fulfilling the XFEL specifications for vector-sum regulation and cavity resonance control. However, the combined use of these two feedback loops still results in system instabilities, which need further investigations.

REFERENCES

[1] J. Sekutowicz *et al.*, "Feasibility of CW and LP Operation of the XFEL Linac", FEL 2013, New York , USA.

[2] J. Sekutowicz *et al.*, "CW and LP operation test of XFEL-like cryomodules", IPAC12, New Orleans,USA, 2012.

[3] J. Sekutowicz *et al.*, "Second CW and LP operation test of XFEL prototype cryomodules", LINAC12 Tel Aviv, Israel, 2012

[4] J. Branlard *et al.*, "The European XFEL LLRF System", IPAC12, New Orleans,USA, 2012.

ISBN 978-3-95450-143-4